1-4-2021

Characterization of the Common Research Model Wing for Low-Fidelity Aerostructural Analysis

Jeffrey D. Taylor
Utah State University

Douglas F. Hunsaker
Utah State University, doug.hunsaker@usu.edu

Recommended Citation

Taylor, J. D. and Hunsaker, D. F., "Characterization of the Common Research Model Wing for Low-Fidelity Aerostructural Analysis," AIAA 2021-1591, AIAA SciTech 2021 Virtual Forum, 11-15 & 19-21 January 2021. doi.org/10.2514/6.2021-1591

Characterization of the Common Research Model Wing for Low-Fidelity Aerostructural Analysis

Jeffrey D. Taylor* and Douglas F. Hunsaker†
Utah State University, Logan, Utah 84322-4130

A characterization of the Common Research Model (CRM) wing for low-fidelity aerostructural optimization is presented. The geometric and structural properties are based on the CAD geometries and finite-element models for the CRM wing and the undeflected Common Research Model Wing (uCRM). Three approximations are presented for the elastic axis from previously-published studies on wing boxes similar to the uCRM, and approximations of the flexural and torsional rigidity are presented from a previously-published study using the uCRM wing. The characterization presented in this paper is intended to be used within low-fidelity aerostructural analysis tools to facilitate rapid design optimization and exploratory studies using the CRM wing.

Nomenclature

$a_{i,b}$ = fit coefficients in the exponential fit for flexural rigidity
$a_{i,cg}$ = fit coefficients in the polynomial fit for section center of gravity
$a_{i,ea}$ = fit coefficients in the polynomial fit for section center of gravity
$a_{i,t}$ = fit coefficients in the exponential fit for torsional rigidity
$a_{\mathrm{L},ijk}$ = fit coefficients in the multidimensional fit for section lift coefficient
$a_{\mathrm{m},ijk}$ = fit coefficients in the multidimensional fit for section moment coefficient
$a_{\mathrm{D},ijk}$ = fit coefficients in the multidimensional fit for section drag coefficient
b = wingspan
C_δ = shape coefficient for the deflection-limited design
C_σ = shape coefficient for the stress-limited design
C_b = fit coefficient in the exponential fit for flexural rigidity
C_D = drag coefficient
C_L = lift coefficient
C_m = moment coefficient
C_t = fit coefficient in the exponential fit for torsional rigidity
c = local wing section chord length
c_{ref} = wing reference chord
c_t = local wing section chord length at the wing tip
D_i = wing induced drag
E = modulus of elasticity of the wing-structure material
G = shear modulus of the wing-structure material
h = spar height of the wing-structure cross-section
I = beam section moment of inertia
J = torsion constant of the wing-structure cross section
M = freestream Mach number
R_A = wing aspect ratio
R_T = wing taper ratio

* PhD Candidate, Mechanical and Aerospace Engineering, 4130 Old Main Hill, AIAA Student Member
† Assistant Professor, Mechanical and Aerospace Engineering, 4130 Old Main Hill, AIAA Senior Member

S = wing planform area
S_{exp} = exposed wing area
S_{ref} = wing reference area
t = panel thickness of the wing-structure
$x_{c/4}$ = x location of the wing-section quarter chord
$z_{c/4}$ = z location of the wing-section quarter chord
ρ = air density
ξ = normalized spanwise coordinate

I. Introduction

THE common research model (CRM)[1] is an open-source aircraft geometry that was developed in 2007-2008 [1] through a partnership between NASA, Boeing, and other industry and government groups for the validation and assessment of computational-fluid-dynamics (CFD) tools [1,2]. The CRM geometry is representative of a typical wide-body transonic transport aircraft. NASA has compiled extensive experimental data for the CRM from at least four wind-tunnel tests [3-5], and several CRM variants have been developed for further study, including a high-lift variant (CRM-HL) [6], a natural laminar flow variant (CRM-NLF) [7-9], and additional variants created by the Office National d'Etudes et de Recherches Aerospaciales (ONERA) [10,11] in France, the Japan Aerospace Exploration Agency (JAXA) [12] in Japan, and the National Research Council (NRC) [13] in Canada.

Aerostructural CRM variants that include a representative wing box have also been presented by Kilmmek [14], Kennedy et al. [15] (QCRM) and Brooks et al. [16] (uCRM-9). Because the CRM was originally developed for aerodynamic validation, the CRM wind-tunnel model wing was designed to match the 1-*g* cruise geometry. However, as pointed out by Keye et al. [17], the wind-tunnel model experiences significant aeroelastic deflection at the cruise condition, which can cause discrepancies between rigid-wing computational results and wind-tunnel data. The aerostructural models presented by Klimmek [14] and Brooks et al. [16] were created to address this concern, and to facilitate analysis of the CRM at multiple flight conditions, including off-design conditions.

In fulfillment of its original purpose, the CRM and its variants have been used in hundreds of high-fidelity CFD studies throughout government, industry, and academia. For example, the CRM was the subject for AIAA CFD drag prediction workshops IV-VI [18-23]. The CRM-HL configuration has been used in AIAA high-lift prediction workshops III and IV and is currently the subject of the AIAA stability and control prediction workshop. The uCRM has been used in several aerostructural and multidisciplinary design optimization studies [16,24]. In addition to benchmarking, the CRM and its variants have also been used as a baseline configuration in studies regarding aircraft icing [25,26], flutter [27], and morphing-wing technologies [28].

Although the CRM was originally intended for validation of high-fidelity CFD tools, it can also provide an excellent benchmark case for the validation of low- to mid-fidelity aerodynamic and aerostructural tools. Low- and mid-fidelity methods also require less computation time than higher-fidelity methods, which makes them ideal for exploratory and proof-of-concept studies. In many cases, these low- and mid-fidelity methods have been shown to be in good agreement with grid-resolved CFD [29-36]. However, to date, there have been very few low- to mid-fidelity studies that use the CRM geometry. This may be, in part, because the publicly-available CRM geometry presents some challenges for many low-fidelity tools. The most apparent challenge is that the official CRM geometry is presented only in initial graphics exchange specification (IGES) and CAD format. The uCRM wing and wing-box geometries are also available in CAD format[2]. In each case, only the outer mold line of the aircraft is given. This is convenient for CFD meshing, but it is not useful for many low-fidelity tools.

It appears that Vassberg et al. [1] give the most detailed description of the full-scale CRM model in their inaugural CRM publication. In this publication, Vassberg et al. [1] present data for the wing leading- and trailing-edge coordinates, twist, chord, thickness-to-chord ratio, max camber, and camber slope at 21 spanwise sections. However, neither the airfoil geometries nor the airfoil performance data is given. This creates a challenge for low-fidelity tools that require 2-D airfoil data for aerodynamic analysis, such as tools based on lifting-line theory [34,37-38]. Moreover, the locus of aerodynamic centers, the quarter-chord-sweep distribution, and the dihedral distribution must be inferred

[1] https://commonresearchmodel.larc.nasa.gov/
[2] http://mdolab.engin.umich.edu/ucrm

or extracted from the CAD geometry. The same is true for the uCRM geometry. The process of extracting the geometric details from the CAD models and other resources often requires significant time and effort.

The purpose of this paper is to present a detailed overview of the CRM and uCRM-9 wing geometries for use in low-fidelity aerodynamic and aerostructural analyses. In the following sections, we describe the geometry of the CRM and uCRM wings and the uCRM wing box, extracted from publicly-available CAD models, and we present an example weight breakdown for the uCRM-9 model for use in aerostructural analyses.

II. Wing Geometry

The coordinate system used in this paper is shown in Fig. 1. The axes are aligned with the conventional body-fixed axes, with the origin at the quarter-chord location of the root airfoil section, as projected to the fuselage centerline. The x-axis is aligned with the horizontal and points out the nose of the aircraft, the y-axis is aligned with the horizontal and points out the right wing, and the z-axis is aligned vertically and points straight down out the bottom of the aircraft, as shown.

The data in this section were extracted from the CAD models for the CRM and uCRM wings using SolidWorks. The CRM wing has a wingspan of $b = 58.76$ m and an aspect ratio of $R_A = 9$. The total wing area is $S = 412.7$ m^2, the reference area is $S_{\text{ref}} = 383.74$ m^2, and the exposed wing area is $S_{\text{exp}} = 337.05$ m^2. The wing is double tapered with a break at 37% semispan and a taper ratio of $R_T = 0.533$ inboard of the break and $R_T = 0.376$ outboard of the break. The reference chord is $c_{\text{ref}} = 7.01$ m. The CRM wing is designed for cruise at $M = 0.85$ at an altitude of 37000 ft (11275 m) and a lift coefficient of $C_L = 0.5$. For standard atmospheric conditions with no temperature offset, this gives a Reynolds number near $\text{Re} = 4.3 \times 10^7$. Wing and flight reference values are summarized in Table 1.

The uCRM wing has the same wingspan and planform shape as the CRM but is designed to represent the undeflected, 0g loading case for the CRM. The uCRM wing also includes a wing box that was designed through a reverse-engineering process and produces the original CRM shape when loaded at cruise. A top-down view of the CRM/uCRM planform is shown in Fig. 2.

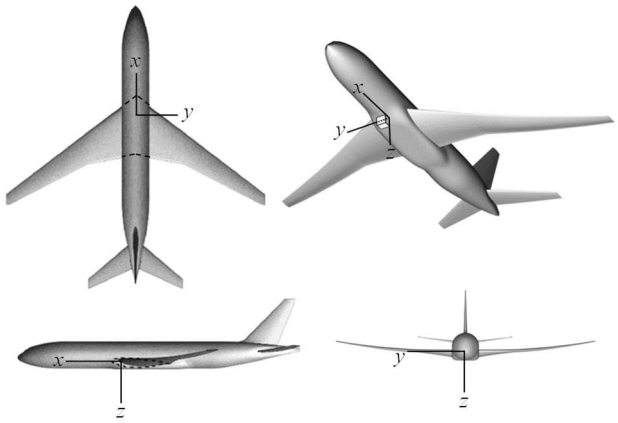

Fig. 1 Coordinate system for the CRM and uCRM wing.

Table 1 Wing and flight reference values for the CRM/uCRM.

wingspan, m	58.76
aspect ratio	9.00
total wing area, m^2	412.70
reference area, m^2	383.74
exposed wing area, m^2	337.05
reference chord, m	7.01
altitude, m	11275.19
Mach number	0.85
lift coefficient	0.50
Reynolds number	4.33×10^7

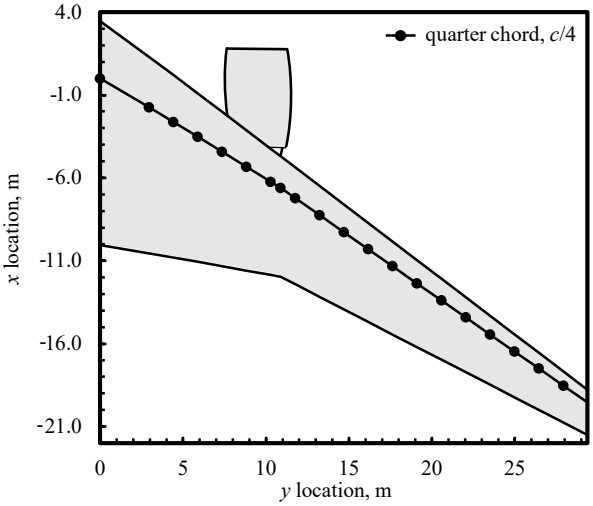

Fig. 2 Planform view of the CRM/uCRM wing geometry.

A. Chord distribution

In Ref. [1], Vassberg et al. give the wing chord distribution, and other wing geometry parameters, at 21 spanwise locations beginning at the wing root and ending at the wing tip. For consistency, the data in this section are shown at the same 21 spanwise locations. The chord was verified from the uCRM CAD geometry by slicing the wing at each spanwise location of interest on a plane parallel to the *x*-axis and perpendicular to the projection of a spline fit through the locus of section quarter-chord points in the *y*-*z* plane. Accounting for the wing twist, the chord was measured from the local airfoil cross-section leading edge to trailing edge. The resulting chord distribution matched the data given by Vassberg et al. [1] for the CRM. The chord distribution is shown in Fig. 3, and values for the local chord at the 21 locations given by Vassberg et al. [1] are given in Table A1 in the appendix.

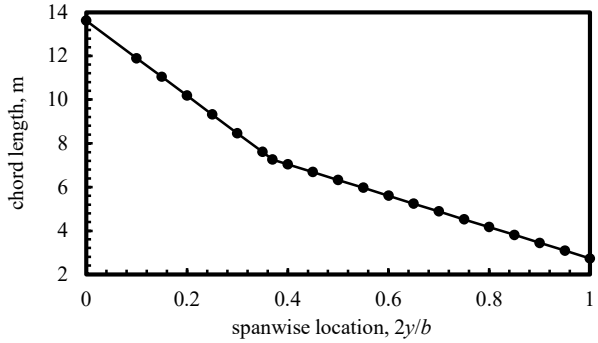

Fig. 3 Chord distribution for the CRM/uCRM wing.

B. Quarter-Chord Sweep

The spanwise variation in quarter-chord sweep for the uCRM and CRM wings is shown in Fig. 4. The sweep angle was extracted from the CAD model by measuring the angle in the *x*-*y* plane between the *y*-axis and a line tangent to the projection in the *x*-*y* plane of the locus of section quarter-chord points at each of the 21 spanwise locations of interest. The results in Fig. 4 show that outboard of the break ($2y/b = 0.37$), the sweep angle is fairly constant at around 35 degrees. Note that the sweep distribution for the CRM at cruise and uCRM at 0*g* have slight differences to account for the effects of bending about the z-axis. However, these differences are small. Values for the sweep distributions of the CRM and uCRM are given in Table A1 in the appendix.

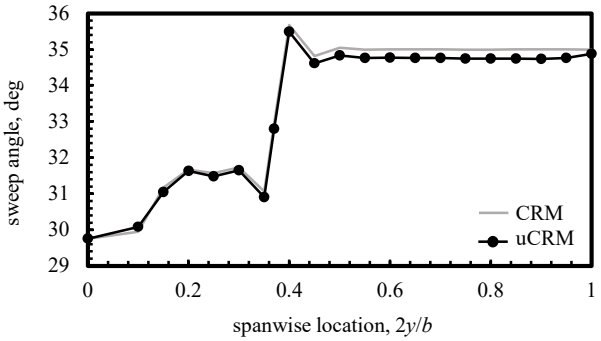

Fig. 4 Spanwise variation in quarter-chord sweep angle for the CRM and uCRM wings.

C. Quarter-Chord dihedral

The dihedral angle was obtained in a manner similar to that used to obtain the quarter-chord sweep angle. However, the dihedral angle at each spanwise section was measured between the *y*-axis and line in the *y*-*z* plane tangent to the projection of the locus of section quarter-chord points in the same plane. The resulting dihedral distributions for the CRM and uCRM wings are shown in Fig. 5. Here, we see that the uCRM dihedral distribution at 0g differs significantly from the CRM dihedral distribution at cruise due to the aeroelastic effects of bending about the *x*-axis. In fact, comparing the deflected 1g CRM geometry to the uCRM at 0g, bending in cruise results in a wingtip deflection of about 2.56 m, or 8.7% semispan. Values for the dihedral distributions for the CRM and uCRM are given in Table A1 in the appendix.

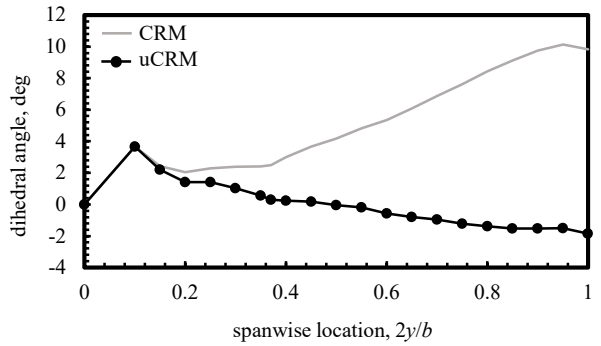

Fig. 5 Spanwise variation in quarter-chord dihedral angle for the CRM and uCRM wings.

D. Wing twist

Figure 6 shows the wing-twist distribution for the CRM and uCRM wings. The wing twist was obtained by measuring the angle between the *x*-axis and the chord of the local airfoil section, which was obtained as described in Section II.A. Figure 5 shows that the twist distribution for the uCRM varies significantly from the CRM twist distribution to account for the effects of aeroelastic twist. The twist distributions for the CRM and uCRM wings are given in Table A1 in the appendix.

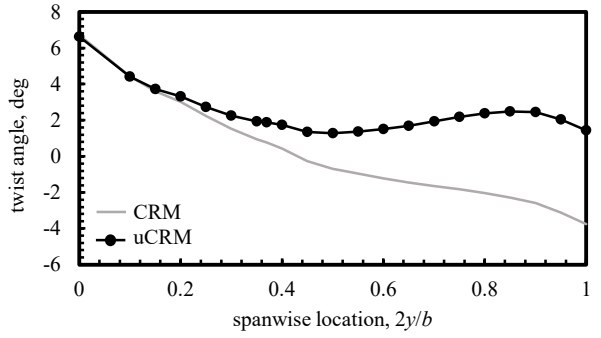

Fig. 6 Wing twist distribution for the CRM and uCRM wings.

E. Section Airfoil properties

Some low-fidelity aerodynamic tools require section aerodynamic properties. In order to obtain these properties, the airfoil section geometric profiles must be known. The airfoil section profiles were obtained from the CRM and uCRM CAD geometries by extracting the intersection curves between the wing surface and the plane parallel to the x-axis and perpendicular to the projection in the y-z plane of a spline fit through the locus of section quarter-chord points. By extracting the airfoil profiles in this manner, the rigid-body rotation of the wing due to bending about the x-axis is preserved, so that the uCRM airfoils and CRM airfoils are consistent. The airfoil stacks for the CRM and uCRM wings are shown in Fig. 7. For better visualization of the airfoils, Fig. 8 shows a schematic of the CRM/uCRM airfoils with zero twist, aligned at the quarter chord location. The coordinates of the airfoil surfaces are available from the Utah State University library repository.[1]

With the airfoil geometric profiles known, the section properties can be obtained using any airfoil analysis tool. In this paper, transonic data for lift coefficient, moment coefficient, and drag coefficient were obtained using the method given by Fujiwara et al. [39], which couples the transonic small-disturbance theory code TSFOIL with an integral boundary-layer method. Data were obtained for a series of angles of attack, Reynolds numbers, and Mach numbers.

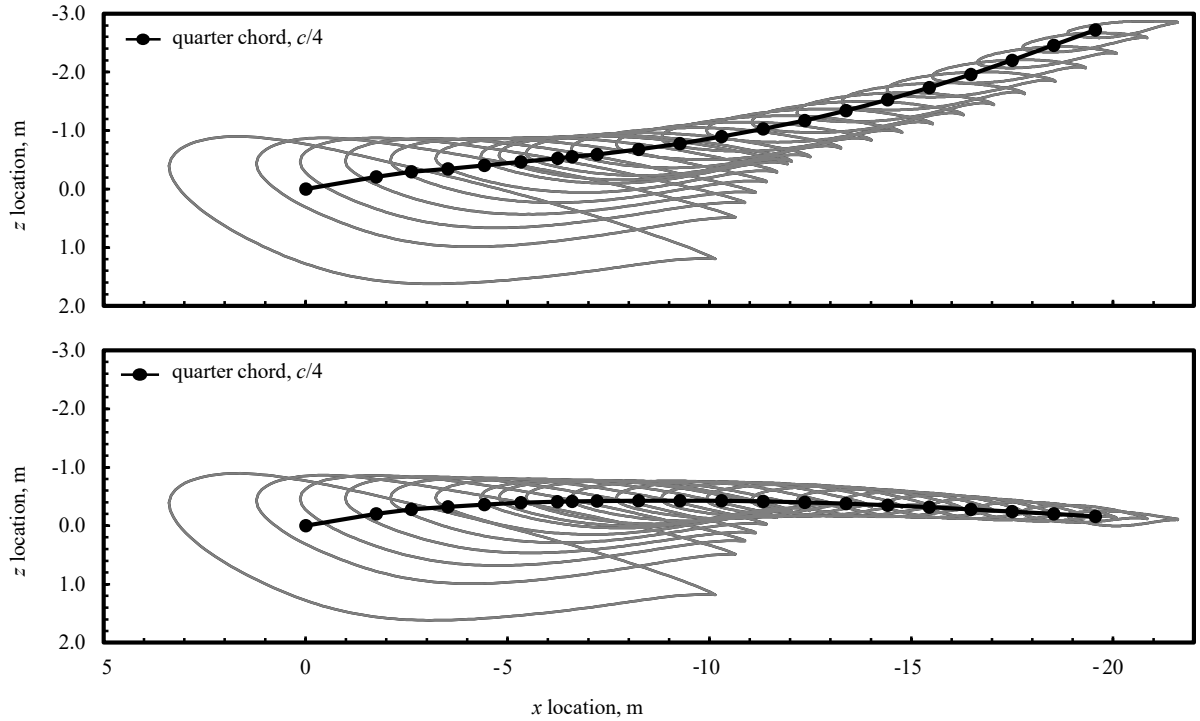

Fig. 7 Airfoil stacks for the CRM wing (top) and the uCRM wing (bottom).

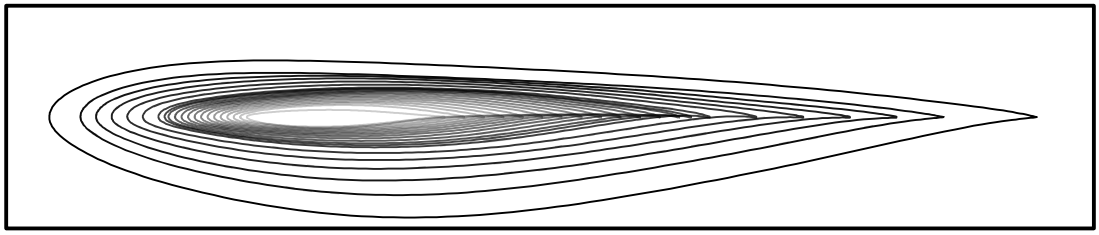

Fig. 8 Schematic of the CRM/uCRM airfoils with zero twist, aligned at the quarter-chord location.

[1] https://digitalcommons.usu.edu/all_datasets/125 (doi: 10.26078/8nv8-yj03)

Full airfoil data is available to the reader through the Utah State University library repository.[2] The method shown by Ullah et al. [40] was used to obtain a series of multi-dimensional curve fits to data for airfoil lift coefficient, drag coefficient, and moment coefficient as a function of angle of attack, Reynolds number, and Mach number. For simplicity, in this paper, we use multidimensional linear fits for the lift coefficient and moment coefficient and multidimensional parabolic fits for the drag coefficient, i.e.,

$$\widetilde{C}_L = \sum_{i=0}^{1}\sum_{j=0}^{1}\sum_{k=0}^{1} a_{L,ijk}\alpha^i \,\mathrm{Re}^j\, M^k \tag{1}$$

$$\widetilde{C}_m = \sum_{i=0}^{1}\sum_{j=0}^{1}\sum_{k=0}^{1} a_{m,ijk}\alpha^i \,\mathrm{Re}^j\, M^k \tag{2}$$

$$\widetilde{C}_D = \sum_{i=0}^{2}\sum_{j=0}^{2}\sum_{k=0}^{2} a_{D,ijk}\alpha^i \,\mathrm{Re}^j\, M^k \tag{3}$$

where $a_{L,ijk}$, $a_{m,ijk}$, are $a_{D,ijk}$ are arrays of fit coefficients, which are given in Tables A2-A6 in the appendix for all of the CRM/uCRM airfoils. For reference, the data and fits for the lift coefficient, moment coefficient, and drag coefficient, as a function of angle of attack, of the break airfoil ($2y/b = 0.37$) at a Reynolds number of $\mathrm{Re} = 3.22\times10^7$ and a Mach number of $M = 0.84$ are shown in Fig. 9.

To give a more intuitive visualization of the spanwise variation in airfoil properties for the CRM and uCRM wings, the spanwise change in the lift slope $\widetilde{C}_{L,\alpha}$ and the coefficient $\widetilde{C}_{L_0}$; the moment parameters $\widetilde{C}_{m,\alpha}$ and $\widetilde{C}_{m_0}$; and the drag parameters $\widetilde{C}_{D_0}$, $\widetilde{C}_{D_L}$, and $\widetilde{C}_{D_{L^2}}$, are shown in Fig. 10. Note that the parameters $\widetilde{C}_{L,\alpha}$ and $\widetilde{C}_{L_0}$ come from the linear approximation for lift as a function of angle of attack, the parameters $\widetilde{C}_{m,\alpha}$ and $\widetilde{C}_{m_0}$ come from the linear approximation for the moment coefficient as a function of angle of attack, whereas coefficients $\widetilde{C}_{D_0}$, $\widetilde{C}_{D_L}$, and $\widetilde{C}_{D_{L^2}}$ come from the parabolic approximation for the drag coefficient as a function of α. Although we have chosen to use linear and low-order fits for the airfoil data in this paper, the methods shown in this subsection can be generalized to obtain higher-order polynomial fits for any of the airfoil data.

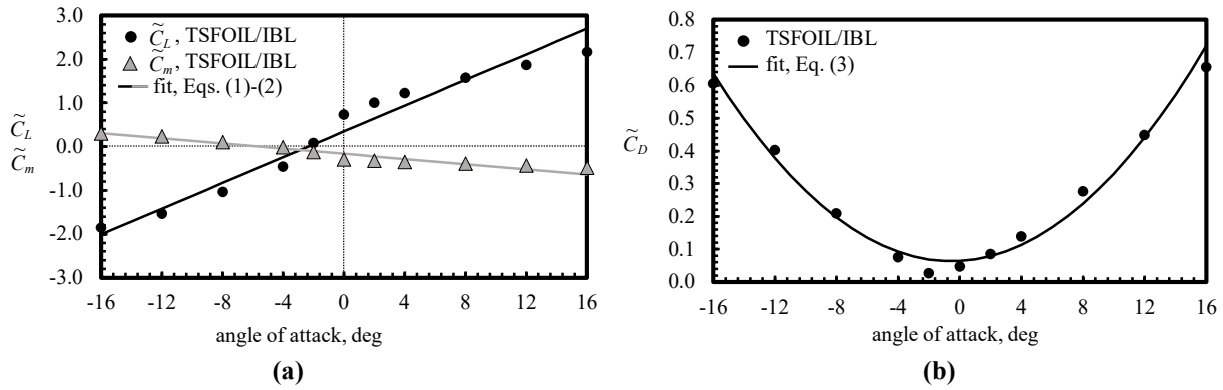

Fig. 9 Airfoil data and polynomial fits for (a) the lift and moment coefficients and (b) the drag coefficient for the break airfoil located at $2y/b = 0.37$ with a Reynolds number of 3.22×10^7 and a Mach number of 0.84

[2] https://digitalcommons.usu.edu/all_datasets/125 (doi: 10.26078/8nv8-yj03)

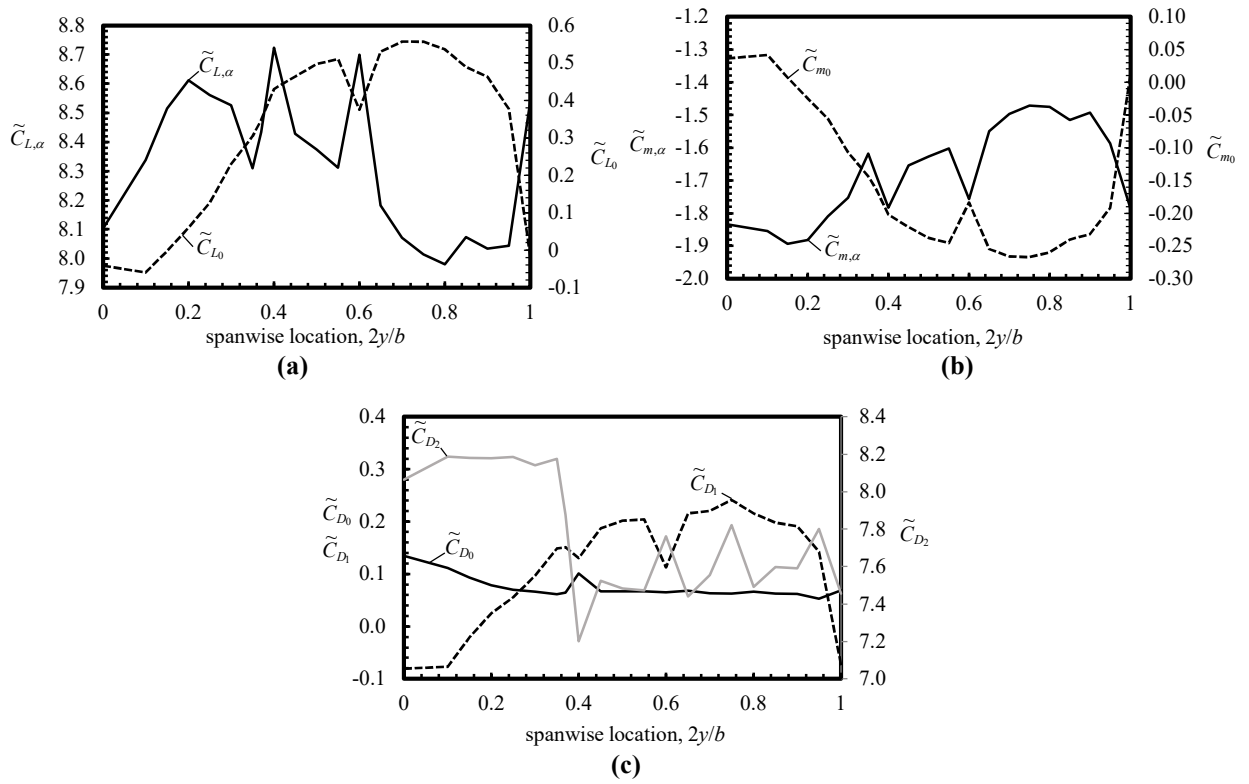

Fig. 10 Section airfoil properties as a function of spanwise location; (a) parameters for the linear approximation of the lift coefficient with respect to angle of attack, (b) parameters for the linear approximation of the moment coefficient with respect to angle of attack, and (c) parameters for the parabolic approximation of the drag coefficient with respect to angle of attack.

III. Wing Box Geometry

The uCRM-9 wing box was designed based on cutaway drawings for the Boeing 777-200ER wing structure and tailored to conform to the CRM 1-g outer mold line [16]. The jig twist for the uCRM geometry was then obtained using an inverse-engineering process, as described by Brooks et al. [16]. The wing box includes upper and lower skins, a front and rear spar, and 49 ribs, placed chordwise along the wing box running length. The data in this section is reported at each of these rib locations. Figure 11 shows a planform view of the wing box and its location within the uCRM wing. A description of the outer dimensions of the wing box, approximations for the center of gravity and the elastic axis, and approximations for the wing flexural and torsional rigidity are given in the following subsections. Note that because the ribs are oriented perpendicular to the wing running length, the y data for the front spar, rear spar, center of gravity, and elastic axis vary slightly in the swept portion of the wingbox. The flexural and torsional rigidity are reported at the y coordinates of the elastic axis. Values for key wing box geometric parameters are shown in Tables A7 and A8 in the appendix.

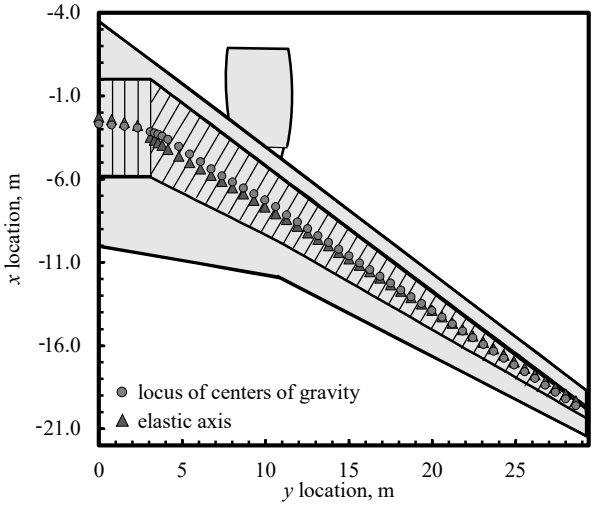

Fig. 11 Planform view of the uCRM-9 wing box as extracted from the CAD geometry.

A. Wing Box Dimensions

The uCRM-9 wingbox includes a leading-edge spar and trailing-edge spar connected by upper and lower panels that conform to the upper and lower wing skins. The wing-box is straight from the root to the fuselage body, which lies at about 10% of the semispan and swept outboard of the fuselage body. Outboard of the fuselage, the leading-edge spar is nearly straight, with a minor kink at the wing break. The trailing-edge spar also has a minor kink at the break. The normalized chordwise location of the leading and trailing-edge spars are shown in Fig. 12 as a function of span.

Because the wing box conforms to the airfoil geometry, the leading- and trailing-edge spars have different heights. Figure 13 shows the normalized spar height for each spar as a function of span. The thicknesses of the wingbox components was obtained from the wing box finite-element file for the uCRM-9, given by the University of Michigan.[3] The thicknesses for the front and rear spars, upper and lower skins, and ribs are shown in Figs. 14, 15, and 16, respectively. Note that due to the change in wing box sweep at 10% semispan, there is no corresponding rear-spar section for ribs 4-6, and rib 4 has four distinct sections, labeled in Fig. 16, in order from front spar to rear spar, as *a*, *b*, *c*, and *d*.

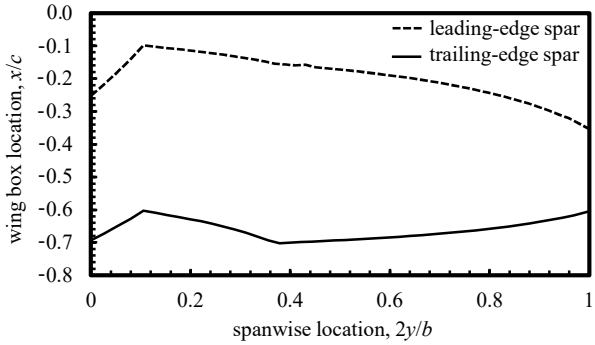

Fig. 12 Normalized chordwise location (measured from the wing leading edge) of the leading- and trailing-edge spars of the uCRM-9 wingbox, as a function of span.

[3] http://mdolab.engin.umich.edu/ucrm

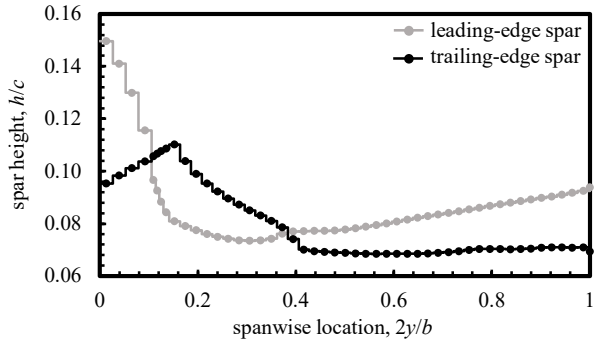

Fig. 13 Normalized spar-height distribution for the leading- and trailing-edge spars of the uCRM-9 wing box.

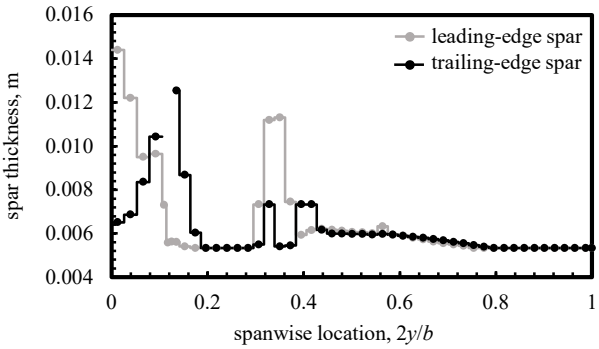

Fig. 14 Thicknesses of the leading- and trailing-edge spars for the uCRM-9 wing box.

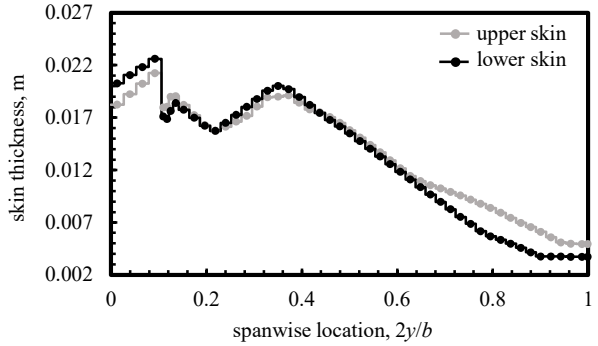

Fig. 15 Thicknesses of the upper and lower skins for the uCRM-9 wing box.

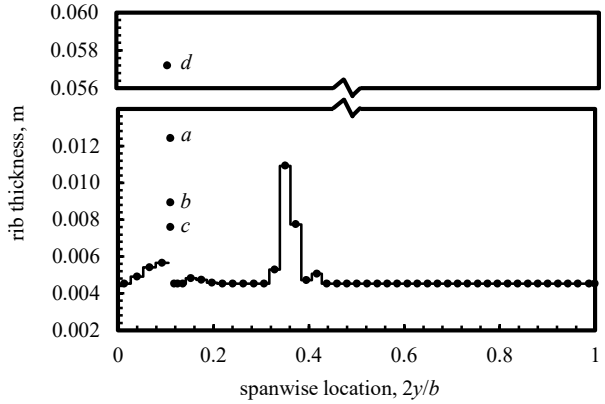

Fig. 16 Thicknesses of the ribs for the uCRM-9 wing box.

B. Locus of Centers of Gravity and Elastic Axis

The locus of section centers of gravity for the uCRM-9 wing box was obtained by extracting the center of gravity of the wing box cross-section from the finite-element model for the uCRM-9 at each spanwise location of interest. The resulting locus of centers of gravity is shown in Fig. 17, normalized by the local chord. For convenience, the normalized data were fit to a polynomial. Because the wing-box geometry is discontinuous at the wing-body junction (10% semispan) and the break (37% semispan), the fits were performed independently on three sections spanning 0-10% semispan, 10-37% semispan, and 37-100% semispan, respectively. The result is a piecewise function of the form

$$\frac{x_{cg}}{c} = \begin{cases} a_{0,cg} + a_{1,cg}\xi & 0 \le \xi \le 0.1 \\ b_{0,cg} + b_{1,cg}\xi + b_{2,cg}\xi^2 + b_{3,cg}\xi^3 & 0.1 < \xi \le 0.37 \\ c_{0,cg} + c_{1,cg}\xi + c_{2,cg}\xi^2 & 0.37 < \xi \le 1.0 \end{cases} \tag{4}$$

where $\xi = 2y/b$ is the normalized spanwise coordinate, and $a_{i,cg}$, $b_{i,cg}$, and $c_{i,cg}$ are the fit coefficients for the center of gravity, which are given in Table 2. The fits are shown with the data in Fig. 17.

For most aerostructural studies, the elastic axis is obtained from FEM models of the wingbox. However, FEM analysis is beyond the scope of this paper. Instead, we show here results from previously-published data for the elastic axis of wings similar to the uCRM-9. The three studies considered here are from Chauhan and Martins [24], Cramer and Nguyen [41], and Stodieck et al. [42]. Chauhan and Martins [24] approximated the elastic axis of the uCRM-9 wingbox in using the weighted-average process described in the previous paragraph. The result is identical to the center of gravity estimate shown in Fig. 17. Cramer and Nguyen [41] approximated the elastic axis for an elastic wind-tunnel model as a straight line with a sweep angle of 31.5 degrees beginning at about 40% of the chord at the wing-body junction. The elastic axis presented by Stodieck et al. [42] was obtained from computational models of an aluminum wing box, designed by the authors for the CRM. The elastic axis from each of these studies is shown in Fig. 18.

Averaging the data from each of these studies gives the data points denoted by black circles in Fig. 18. Using the same wing partitions as shown in Eq. (4), the normalized average elastic-axis data were fit to a piecewise function of the form

$$\frac{x_{ea}}{c} = \begin{cases} a_{0,ea} + a_{1,ea}\xi & 0 \le \xi \le 0.1 \\ b_{0,ea} + b_{1,cg}\xi + b_{2,ea}\xi^2 + b_{3,ea}\xi^3 + b_{4,ea}\xi^4 & 0.1 < \xi \le 0.37 \\ c_{0,ea} + c_{1,ea}\xi + c_{2,ea}\xi^2 & 0.37 < \xi \le 1.0 \end{cases} \tag{5}$$

Here, the coefficients $a_{i,ea}$, $b_{i,ea}$, and $c_{i,ea}$ are fit coefficients for the elastic axis, and are given in Table 2. The resulting fit is shown alongside the data in Fig. 18.

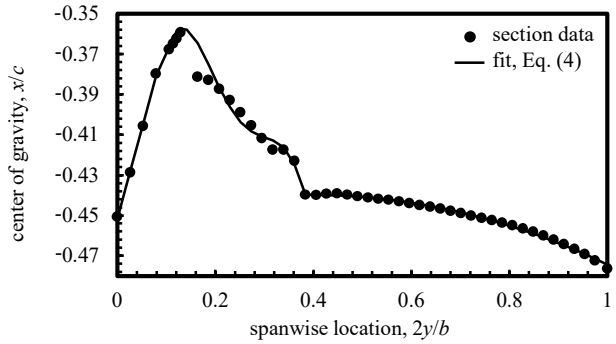

Fig. 17 Approximate normalized chordwise location (measured from the wing leading edge) of the center of gravity for the uCRM-9 wingbox.

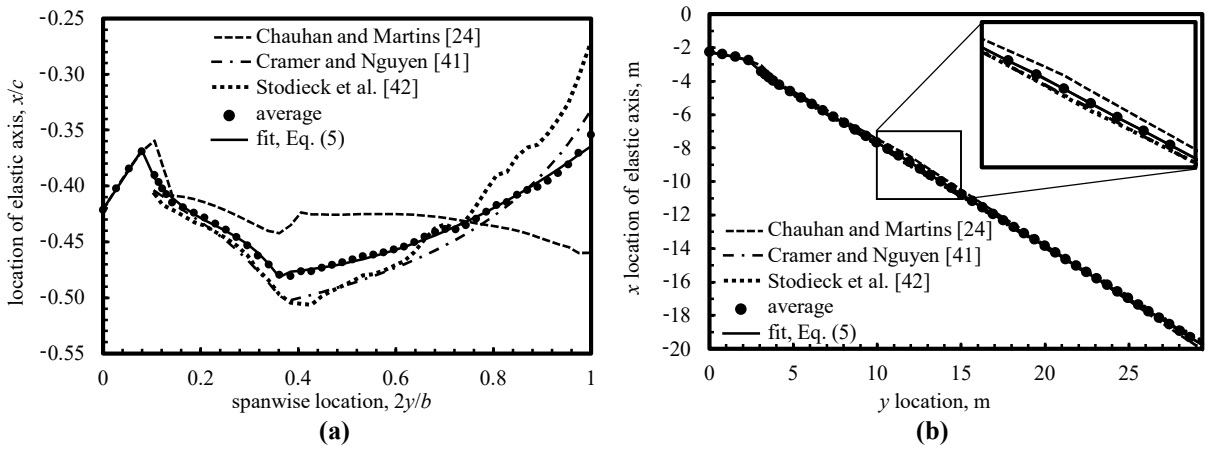

Fig. 18 Approximate locations of the uCRM-9 elastic axis in (a) normalized chordwise coordinates (measured from the wing leading edge) and (b) dimensional coordinates.

Table 2 Fit coefficients for the piecewise approximations of the locus of normlized centers of gravity and elastic axis (measured from the wing leading edge) of the uCRM-9 wing box.

center of gravity, $x_{cg}/c(\xi)$		elastic axis, $x_{ea}/c(\xi)$	
$a_{0,cg}$	0.4206	$a_{0,ea}$	0.4516
$a_{1,cg}$	-0.6640	$a_{1,ea}$	-0.8940
$b_{0,cg}$	0.2928	$b_{0,ea}$	0.7584
$b_{1,cg}$	1.4144	$b_{1,ea}$	-8.1124
$b_{2,cg}$	-5.1770	$b_{2,ea}$	56.8562
$b_{3,cg}$	7.4934	$b_{3,ea}$	-160.9238
		$b_{4,ea}$	162.2804
$c_{0,cg}$	0.4591	$c_{0,ea}$	0.4552
$c_{1,cg}$	0.1335	$c_{1,ea}$	-0.0771
$c_{2,cg}$	-0.2283	$c_{2,ea}$	0.0963

C. Flexural and Torsional Rigidity

The approximate flexural and torsional rigidity for the uCRM model were obtained from data presented by Fujiwara et al. [28]. In their study, Fujiwara et al. [28] presented the flexural and torsional rigidity required to produce the CRM 1-g geometry from their version of the uCRM model. The data shown in Fig. 19 were reproduced from this study. As was done for the center of gravity and elastic axis, the flexural and torsional rigidity were fit to a function. However, here, the fits were performed on the data within the range $0.1 \le \xi \le 1.0$. Below $\xi = 0.1$ the data were linearly interpolated to account for the dip shown in Fig. 19. The results are expressions for the flexural and torsional rigidity of the form

$$EI = C_b e^{a_{0,b} - a_{1,b}\xi} \tag{6}$$

$$GJ = C_t e^{a_{0,t} - a_{1,t}\xi} \tag{7}$$

where C_b, and $a_{0,b}$ and $a_{1,b}$ are fit coefficients for the flexural rigidity, and C_t, and $a_{0,t}$ and $a_{1,t}$ are fit coefficients for the torsional rigidity. Values for each of these coefficients are given in Table 3, and the fits are shown alongside the respective data in Fig. 19.

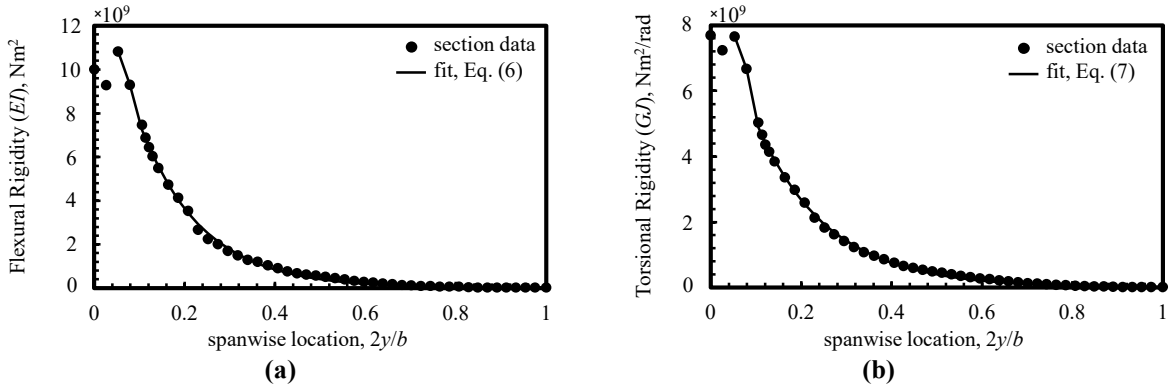

Fig. 19 Flexural Rigidity and Torsional Rigidity as a function of span for the uCRM-9 wing box. Reproduced from Fujiwara et al. [28]

Table 3 Fit coefficients for the approximate expressions for the flexural and torsional rigidity for the uCRM-9 wing structure.

Flexural Rigidity, $EI(\xi)$		Torsional Rigidity, $GJ(\xi)$	
C_b	100.3820	C_t	104.9792
$a_{0,b}$	18.8684	$a_{0,t}$	18.3235
$a_{1,b}$	7.3045	$a_{1,t}$	6.3429

IV. Weight Distribution

Key weight characteristics for the uCRM-9 can be obtained from data presented by Brooks et al. [16] and from publicly-available data for the Boeing 777-200ER [43], upon which the uCRM geometry is partially based. A summary of the weight breakdown is given in Table 4. Note that in this paper, we assume that the CRM carries one engine weighing 7,893 kg on each wing. The cruise weight is found from the nominal flight condition described at the beginning of Section II. Assuming that the CRM operates in steady level flight with 50% fuel at the nominal flight condition, the CRM weight with 50% fuel is found from the lift coefficient to be 220,240 kg. The weight with 100% fuel is then found by adding half of the maximum usable fuel weight (137,460 kg) for the Boeing 777-200ER [43] to give 288,970 kg, which is below the maximum takeoff weight (MTOW) of 297,550 kg [43]. The "net" weight in Table 4 is the total CRM weight with 100% fuel less the wing-structure weight, which is approximated using the method described below. The root weight is the net weight minus the total fuel load and the weight of both engines.

Table 4 Weight characteristics for the uCRM configuration.

Maximum Takeoff Weight (MTOW), kg	297,550
Maximum Zero-Fuel Weight (MZFW), kg	195,040
Operational Empty Weight (OEW), kg	138,100
Cruise Weight (50% Fuel), kg	220,240
Total Weight (100% Fuel), kg	288,970
Design Payload, kg	34,000
Usable Fuel Weight, kg	137,460
Root Weight, kg	105,806
Net Weight (100% Fuel), kg	259,052
Engine Weight, kg	7,893
Wing-Structure Weight, kg	29,895

For the low-fidelity CRM model, the wing-structure weight distribution was extracted from the uCRM-9 wing box finite element model. The material properties were chosen to be typical of 7000-series aluminum, as shown in Table 5. The resulting wing-structure weight distribution is shown in Fig. 20, without the weight of the ribs. Using the volume from the uCRM-9 wing box finite element model, including the ribs, and the density shown in Table 5, the total wing-structure weight is 23,916 kg, which matches the value found by Brooks et al. [16]. As suggested by Brooks et al. [16], we obtain the final wing-structure weight by multiplying this value by 1.25 to account for the weight of fasteners, overlaps, and other unmodeled structural components. The result is a final wing-structure weight of 29,895 kg, as reported in Table 4.

The net weight distribution is defined as the distribution of all non-structural components carried by the wing. Here, we assume that the majority of net weight consists of the fuel weight and the weight of the engines, which are mounted at about 32.7% of the semispan [43]. The approximate fuel model for the low-fidelity uCRM is based on publicly-available data for the Boeing 777-200ER [43,44]. As seen in Table 4, the maximum usable fuel weight is 137,460 kg. Based on fuel-tank layout diagrams for the Boeing 777-200ER [44], we assume that 57.7% of the fuel is carried in a center tank and 42.3% is carried in wing tanks. Assuming that the fuel density is 803.1 kg/m^3, and assuming that the fuel tanks fill the volume of the wing box, we find that in order to carry their respective portions of the fuel weight, the center tank must extend to about 21% of the wing semispan, and the wing tank must extend from 21% semispan to 76% semispan. The fuel-tank layout is shown in Fig. 21. Over the course of a flight, fuel is first burned from the center tank, after which, fuel is burned from the wing tanks. Thus, as the fuel burns, the fuel-weight distribution changes, as shown in Fig. 22. Note that Fig. 22 also includes the weight of the engine in the net-weight distribution. The thrust-specific fuel consumption is estimated to be $c_T = 0.054$ kg/(N h).

Table 5 Material properties used for the low-fidelity CRM wing-structure weight estimation.

Density, kg/m^3	2780
Specific Weight, kg/(m^{2}s^2)	27,272
Modulus of Elasticity, Pa	7.31×10^{10}
Yield Strength, Pa	4.2×10^{8}
Poisson Ratio	0.33
Shear Modulus, Pa	2.75×10^{10}

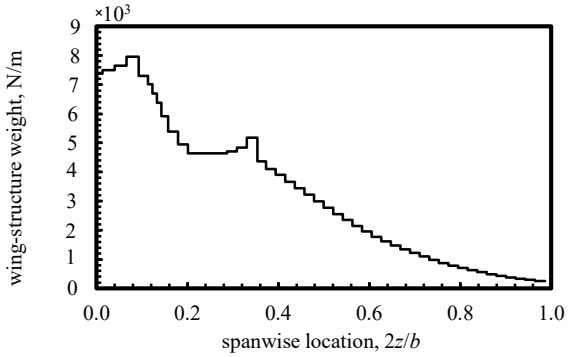

Fig. 20 Approximate wing-structure weight distribution for the CRM wing.

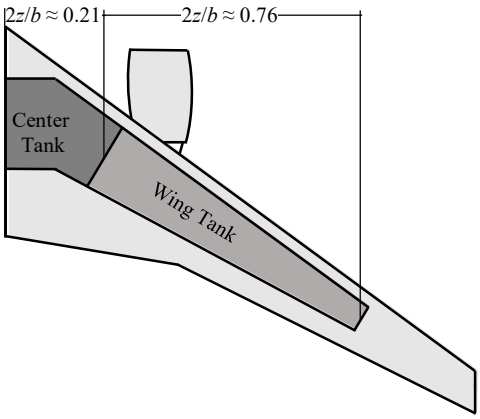

Fig. 21 Schematic of an example fuel-tank layout for the CRM.

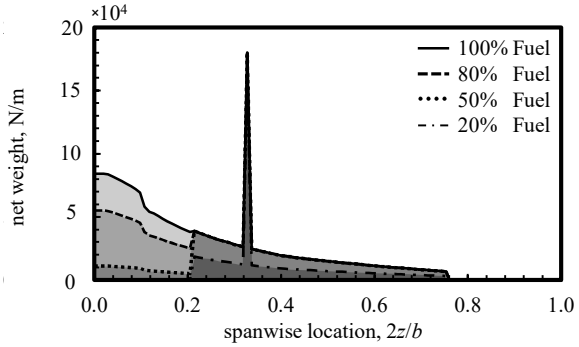

Fig. 22 Example net-weight distributions for the CRM.

V. Conclusion

The CRM was designed as a benchmark geometry for high-fidelity CFD methods, and it and its variants have been used in hundreds of high-fidelity studies throughout government, academia, and industry. The uCRM-9 geometry is an aerostructural variant of the CRM that includes a wing box model and an outer mold line representative of the 0-g geometry of the CRM. Although both the CRM and uCRM-9 are tailored for high-fidelity studies, they can also be used with low-fidelity models as a benchmark configuration for exploratory and proof-of-concept studies that require a high number of computations. However, most low fidelity methods require parameterized data of the geometry to be used. Extracting these data is often difficult and time consuming. Therefore, in this paper, we have presented a characterization of the CRM/uCRM-9 wing and the uCRM-9 wing box that includes geometric and weight data that can be used with low-fidelity aerostructural analysis tools.

The wing outer mold line geometry was extracted from CAD models of the CRM and uCRM-9 wings. The chord distribution, sweep distribution, dihedral distribution, and twist distribution are shown in Figs. 3-6. A summary of the wing properties and geometric distributions is given in Table A1 in the appendix. The airfoil profiles were also extracted from the CAD geometries and are shown in Figs. 7 and 8. Transonic data for the lift coefficient, moment coefficient, and drag coefficient for each airfoil were obtained using the transonic small-disturbance theory code TSFOIL in conjunction with an integral boundary layer method, as described in Section II.E. The data were obtained over a range of angles of attack, Reynolds numbers, and Mach numbers. Fit coefficients for the multidimensional linear fits of lift coefficient and moment coefficient with respect to each of these variables are shown in Tables A2 and A3. Fit coefficients for the multidimensional parabolic fits of drag coefficient with respect to the same variables are given in Tables A4-A6.

The wing box geometry was extracted from CAD and finite-element models of the uCRM-9 wing box. A geometric description of the wing box, including its location within the wing and dimensions and thicknesses of the various wing box components, is given in Section III.A. The spar locations, spar heights, and wing box component thicknesses are given in Fig. 12, Fig. 13, and Figs. 14-16, respectively. The locus of aerodynamic centers was also obtained from the

finite element model of the uCRM-9 wing box and is shown in Fig. 17. Obtaining the elastic axis for the uCRM-9 wing is beyond the scope of this study. Therefore, three approximations for the elastic axis from previously-published studies on wing similar to the uCRM-9 are shown in Fig. 18, along with the average of the three approximations. Similarly, approximations for the flexural and torsional rigidity were obtained from previously-published data, as shown in Fig. 19.

Section IV shows the weight breakdown of the uCRM-9 wing, based on available data on the Boeing 777-200ER and data from the University of Michigan. The structural weight distribution, without the ribs, is shown in Fig. 20. An example fuel model is also presented, based, in part, on available fuel data for the 777-200ER. The resulting net-weight distribution resulting from this model is shown in Fig. 22. It is anticipated that the low-fidelity characterization of the CRM/uCRM wing presented in this paper will be useful for low-fidelity aerostructural analysis and optimization of the CRM configuration.

Appendix

Table A1 Planform, twist, dihedral, and sweep information for the CRM and uCRM wing geometries.

		CRM					uCRM				
ξ	chord, m	twist, deg	$x_{c/4}$, m	$z_{c/4}$, m	dihedral, deg	sweep, deg	twist, deg	$x_{c/4}$, m	$z_{c/4}$, m	dihedral, deg	sweep, deg
0.00	13.6161	6.7166	0.0000	0.0000	0.0000	29.7522	6.6338	0.0000	0.0000	0.0000	29.7522
0.10	11.8976	4.4402	1.7486	-0.2084	3.6709	29.9501	4.4145	1.7482	-0.2006	3.6709	30.0793
0.15	11.0384	3.6063	2.6197	-0.2934	2.4339	31.1690	3.7304	2.6188	-0.2785	2.2160	31.0457
0.20	10.1790	3.0131	3.5216	-0.3466	2.0360	31.6678	3.3105	3.5203	-0.3199	1.4119	31.6328
0.25	9.3197	2.2419	4.4283	-0.4032	2.2941	31.5728	2.7349	4.4268	-0.3580	1.4162	31.4833
0.30	8.4604	1.5252	5.3324	-0.4628	2.3945	31.7263	2.2480	5.3310	-0.3894	1.0428	31.6504
0.35	7.6010	0.9379	6.2367	-0.5254	2.4187	31.0666	1.9361	6.2353	-0.4106	0.5650	30.9032
0.37	7.2573	0.7635	6.5982	-0.5504	2.5002	32.9494	1.8787	6.5968	-0.4152	0.3120	32.8045
0.40	7.0416	0.4285	7.2154	-0.5923	3.0022	35.6796	1.7370	7.2141	-0.4186	0.2433	35.4894
0.45	6.6821	-0.2621	8.2440	-0.6796	3.6606	34.8209	1.3592	8.2430	-0.4263	0.1905	34.6167
0.50	6.3226	-0.6782	9.2724	-0.7791	4.1806	35.0526	1.2762	9.2716	-0.4268	-0.0358	34.8329
0.55	5.9631	-0.9436	10.3009	-0.8954	4.8250	34.9914	1.3784	10.3001	-0.4249	-0.1792	34.7655
0.60	5.6035	-1.2067	11.3293	-1.0261	5.3523	35.0048	1.5129	11.3286	-0.4154	-0.5727	34.7735
0.65	5.2440	-1.4526	12.3578	-1.1722	6.0639	35.0039	1.6816	12.3570	-0.3970	-0.7911	34.7685
0.70	4.8845	-1.6350	13.3863	-1.3388	6.8534	35.0048	1.9304	13.3855	-0.3753	-0.9495	34.7653
0.75	4.5250	-1.8158	14.4147	-1.5250	7.6114	34.9974	2.1837	14.4139	-0.3474	-1.2104	34.7518
0.80	4.1654	-2.0301	15.4429	-1.7318	8.4165	34.9986	2.3788	15.4421	-0.3141	-1.3639	34.7448
0.85	3.8059	-2.2772	16.4713	-1.9586	9.1030	35.0031	2.4860	16.4706	-0.2774	-1.5117	34.7463
0.90	3.4464	-2.5773	17.4997	-2.2021	9.7474	35.0034	2.4437	17.4992	-0.2377	-1.5156	34.7378
0.95	3.0869	-3.1248	18.5280	-2.4608	10.1231	35.0020	2.0515	18.5281	-0.1998	-1.4942	34.7657
1.00	2.7274	-3.7500	19.5560	-2.7207	9.8390	34.9949	1.4465	19.5567	-0.1578	-1.8418	34.8792

Table A2 Multidimensional linear fit coefficients for the lift coefficient produced by the airfoil sections of the CRM/uCRM wing as a function of angle of attack, Mach number, and Reynolds number.

	$a_{L,000}$	$a_{L,001}$	$a_{L,010} \times 10^7$	$a_{L,011} \times 10^7$	$a_{L,100}$	$a_{L,101}$	$a_{L,110}$	$a_{L,111} \times 10^7$
$\xi = 0.0$	-0.5682	0.6200	0.0000	0.0000	17.9513	-11.5657	0.0000	-0.3167
$\xi = 0.1$	-0.5122	0.5225	0.0000	0.0000	16.6136	-9.6691	0.0000	-0.5619
$\xi = 0.15$	-0.2953	0.3401	0.0000	0.0000	15.8984	-8.5657	0.0000	-0.5623
$\xi = 0.2$	-0.1624	0.2535	0.0000	0.0000	14.5488	-6.8159	0.0000	-0.6538
$\xi = 0.25$	-0.0191	0.1564	0.0000	0.0000	14.2191	-6.4702	0.0000	-0.6588
$\xi = 0.3$	0.1917	0.0405	0.0000	0.0000	13.9930	-6.2138	0.0000	-0.8402
$\xi = 0.35$	0.3995	-0.1062	0.0000	0.0000	14.6710	-7.2700	0.0000	-1.0286
$\xi = 0.37$	0.4055	-0.0629	0.0000	0.0000	13.5411	-5.6631	0.0000	-1.1746
$\xi = 0.4$	0.3910	0.0604	0.0000	0.0000	11.6430	-2.9371	0.0000	-1.1959
$\xi = 0.45$	0.4536	0.0346	0.0000	0.0000	12.4849	-4.2587	0.0000	-1.3269
$\xi = 0.5$	0.5343	-0.0163	0.0000	0.0000	12.3558	-4.1372	0.0000	-1.3607
$\xi = 0.55$	0.6403	-0.1218	0.0000	0.0000	12.6962	-4.5681	0.0000	-1.5118
$\xi = 0.6$	0.7591	-0.4458	0.0000	0.0000	14.1389	-6.0314	0.0000	-0.3449
$\xi = 0.65$	0.6512	-0.0900	0.0000	-0.1144	12.8697	-4.8439	0.0000	-1.7401
$\xi = 0.7$	0.6401	-0.0513	0.1078	-0.1431	12.9864	-5.0611	0.0000	-1.9190
$\xi = 0.75$	0.6826	-0.0936	0.1275	-0.1692	13.0417	-5.1567	0.0000	-1.9620
$\xi = 0.8$	0.6481	-0.0800	0.1199	-0.1592	12.8176	-4.7793	0.0000	-2.1277
$\xi = 0.85$	0.5828	-0.0685	0.0000	-0.1312	12.1771	-3.9081	0.0000	-2.1490
$\xi = 0.9$	0.4479	0.0543	0.1226	-0.1573	11.8963	-3.4408	0.0000	-2.4484
$\xi = 0.95$	0.3823	-0.0065	0.1020	-0.1213	11.5509	-2.8649	0.0000	-3.3893
$\xi = 1.0$	-0.1634	0.0953	0.0000	0.0000	9.8103	-0.3978	0.0000	-2.2602

Table A3 Multidimensional linear fit coefficients for the moment coefficient produced by the airfoil sections of the CRM/uCRM wing as a function of angle of attack, Mach number, and Reynolds number.

	$a_{m,000}$	$a_{m,001}$	$a_{m,010}$	$a_{m,011}$	$a_{m,100}$	$a_{m,101}$	$a_{m,110} \times 10^7$	$a_{m,111} \times 10^7$
$\xi = 0.0$	0.0812	-0.0508	0.0000	0.0000	0.9662	-3.4029	-0.1503	0.2010
$\xi = 0.1$	0.0691	-0.0270	0.0000	0.0000	1.4133	-3.9689	-0.2155	0.2819
$\xi = 0.15$	0.0429	-0.0384	0.0000	0.0000	1.6716	-4.3351	-0.1975	0.2640
$\xi = 0.2$	0.0366	-0.0686	0.0000	0.0000	2.0827	-4.8171	-0.2060	0.2765
$\xi = 0.25$	0.0373	-0.1051	0.0000	0.0000	2.1343	-4.7903	-0.1977	0.2658
$\xi = 0.3$	0.0358	-0.1704	0.0000	0.0000	2.1116	-4.7034	-0.2533	0.3344
$\xi = 0.35$	0.0034	-0.1788	0.0000	0.0000	1.7029	-4.0720	-0.3182	0.4160
$\xi = 0.37$	0.0257	-0.2308	0.0000	0.0000	2.0679	-4.6199	-0.3125	0.4192
$\xi = 0.4$	0.0489	-0.3027	0.0000	0.0000	2.4463	-5.1866	-0.2526	0.3487
$\xi = 0.45$	0.0447	-0.3240	0.0000	0.0000	2.1015	-4.6356	-0.2864	0.3929
$\xi = 0.5$	0.0347	-0.3319	0.0000	0.0000	2.1297	-4.6489	-0.3022	0.4155
$\xi = 0.55$	0.0171	-0.3219	0.0000	0.0000	2.0244	-4.5160	-0.3584	0.4890
$\xi = 0.6$	-0.0805	-0.1333	0.0000	0.0000	1.8123	-4.4083	0.0000	0.1380
$\xi = 0.65$	0.0200	-0.3453	0.0000	0.0000	1.8812	-4.3116	-0.3905	0.5359
$\xi = 0.7$	0.0311	-0.3680	0.0000	0.0000	1.8485	-4.2271	-0.4750	0.6417
$\xi = 0.75$	0.0197	-0.3589	0.0000	0.0000	1.7854	-4.1353	-0.4755	0.6466
$\xi = 0.8$	0.0153	-0.3430	0.0000	0.0000	1.8318	-4.2358	-0.4454	0.6232
$\xi = 0.85$	0.0151	-0.3151	0.0000	0.0000	2.1351	-4.6335	-0.4886	0.6714
$\xi = 0.9$	0.0430	-0.3330	0.0000	0.0000	2.1912	-4.7459	-0.4881	0.6931
$\xi = 0.95$	0.0200	-0.2460	0.0000	0.0000	2.4578	-5.1924	-0.6767	0.9233
$\xi = 1.0$	-0.0162	0.0536	0.0000	0.0000	2.9536	-5.9138	-0.3814	0.5391

Table A4 Fit coefficients for the α^0 terms in the multidimensional parabolic fit for the drag coefficient produced by the airfoil sections of the CRM/uCRM wing as a function of angle of attack, Mach number, and Reynolds number.

	$a_{D,000}$	$a_{D,001}$	$a_{D,002}$	$a_{D,010}\times10^7$	$a_{D,011}\times10^7$	$a_{D,012}\times10^7$	$a_{D,020}$	$a_{D,021}$	$a_{D,022}$
$\xi = 0.0$	-0.3249	0.4505	0.1282	0.1428	-0.3937	0.2596	0.0000	0.0000	0.0000
$\xi = 0.1$	-0.1666	0.0736	0.3187	0.1303	-0.3663	0.2444	0.0000	0.0000	0.0000
$\xi = 0.15$	-0.0016	-0.3656	0.5776	0.1648	-0.4587	0.3072	0.0000	0.0000	0.0000
$\xi = 0.2$	0.0985	-0.6075	0.7063	0.1787	-0.4872	0.3196	0.0000	0.0000	0.0000
$\xi = 0.25$	0.1386	-0.6857	0.7275	0.1889	-0.5273	0.3541	0.0000	0.0000	0.0000
$\xi = 0.3$	0.1824	-0.7615	0.7473	0.0000	-0.2667	0.1812	0.0000	0.0000	0.0000
$\xi = 0.35$	0.2710	-0.9996	0.8964	0.0000	0.1840	-0.1239	0.0000	0.0000	0.0000
$\xi = 0.37$	0.1886	-0.7740	0.7525	0.1716	-0.4776	0.3199	0.0000	0.0000	0.0000
$\xi = 0.4$	-6.3579	18.4320	-13.0157	8.6931	-25.2829	17.9795	0.0000	0.0000	0.0000
$\xi = 0.45$	0.0336	-0.3156	0.4274	0.4223	-1.2122	0.8444	0.0000	0.0000	0.0000
$\xi = 0.5$	0.3539	-1.2428	1.0813	0.0000	0.1835	-0.1293	0.0000	0.0000	0.0000
$\xi = 0.55$	0.3909	-1.3550	1.1635	0.0000	0.2156	-0.1511	0.0000	0.0000	0.0000
$\xi = 0.6$	0.2268	-0.8302	0.7671	0.1170	-0.4489	0.3666	0.0000	0.0000	0.0000
$\xi = 0.65$	0.2699	-1.0076	0.9283	0.1245	-0.3463	0.2242	0.0000	0.0000	0.0000
$\xi = 0.7$	-0.0721	-0.0040	0.2055	0.7014	-2.0130	1.4059	0.0000	0.0000	0.0000
$\xi = 0.75$	0.0143	-0.2529	0.3815	0.6093	-1.7422	1.2097	0.0000	0.0000	0.0000
$\xi = 0.8$	0.1697	-0.7273	0.7321	0.3889	-1.0702	0.7154	0.0000	0.0000	0.0000
$\xi = 0.85$	0.2188	-0.8469	0.7993	0.3805	-1.0834	0.7451	0.0000	0.0000	0.0000
$\xi = 0.9$	0.2261	-0.8748	0.8224	0.3380	-0.9252	0.6139	0.0000	0.0000	0.0000
$\xi = 0.95$	0.2908	-1.0783	0.9584	0.3528	-1.0519	0.7431	0.0000	0.0000	0.0000
$\xi = 1.0$	0.5669	-1.8816	1.5356	-0.1123	0.2966	-0.2110	0.0000	0.0000	0.0000

Table A5 Fit coefficients for the α^1 terms in the multidimensional parabolic fit for the drag coefficient produced by the airfoil sections of the CRM/uCRM wing as a function of angle of attack, Mach number, and Reynolds number.

	$a_{D,100}$	$a_{D,101}$	$a_{D,102}$	$a_{D,110}\times10^7$	$a_{D,111}\times10^7$	$a_{D,112}\times10^7$	$a_{D,120}$	$a_{D,121}$	$a_{D,122}$
$\xi = 0.0$	3.4522	-9.5715	6.3852	-0.3702	0.7616	-0.3849	0.0000	0.0000	0.0000
$\xi = 0.1$	3.7241	-10.5048	7.1116	-0.2785	0.6081	-0.3319	0.0000	0.0000	0.0000
$\xi = 0.15$	2.3719	-6.7957	4.6910	-0.2334	0.5091	-0.2763	0.0000	0.0000	0.0000
$\xi = 0.2$	1.8475	-5.0214	3.3820	-0.5856	1.3866	-0.8163	0.0000	0.0000	0.0000
$\xi = 0.25$	1.7373	-4.3757	2.8109	-1.0672	2.6945	-1.6907	0.0000	0.0000	0.0000
$\xi = 0.3$	0.3988	-0.2622	-0.1073	0.2670	-0.7818	0.5436	0.0000	0.0000	0.0000
$\xi = 0.35$	-0.6120	3.0560	-2.5606	0.0000	0.2133	-0.1314	0.0000	0.0000	0.0000
$\xi = 0.37$	-0.5310	2.9002	-2.4828	-0.5517	1.4372	-0.9284	0.0000	0.0000	0.0000
$\xi = 0.4$	7.2507	-19.4816	13.4060	-11.4235	32.7342	-23.0312	0.0000	0.0000	0.0000
$\xi = 0.45$	-2.0364	7.5068	-5.7658	0.3047	-0.8602	0.5854	0.0000	0.0000	0.0000
$\xi = 0.5$	-2.3027	8.3959	-6.4317	-0.1408	0.4136	-0.2967	0.0000	0.0000	0.0000
$\xi = 0.55$	-2.8246	10.1164	-7.7435	0.0000	0.1733	-0.1277	0.0000	0.0000	0.0000
$\xi = 0.6$	-0.1861	2.4692	-2.5041	-0.2853	0.6275	-0.3560	0.0000	0.0000	0.0000
$\xi = 0.65$	-2.2169	8.4434	-6.5833	-1.5703	4.5294	-3.1899	0.0000	0.0000	0.0000
$\xi = 0.7$	-3.0602	10.8701	-8.2789	-0.8040	2.2813	-1.5773	0.0000	0.0000	0.0000
$\xi = 0.75$	-1.6789	6.8642	-5.4344	-3.6051	10.5826	-7.5465	0.0000	0.0000	0.0000
$\xi = 0.8$	-2.7125	9.8408	-7.5601	-0.9386	2.8840	-2.1176	0.0000	0.0000	0.0000
$\xi = 0.85$	-2.2931	8.4391	-6.5175	-0.2211	0.5277	-0.3305	0.0000	0.0000	0.0000
$\xi = 0.9$	-1.4576	5.5134	-4.2259	-1.2781	3.7967	-2.7297	0.0000	0.0000	0.0000
$\xi = 0.95$	-0.9530	4.0416	-3.2442	-0.6794	1.8443	-1.2332	0.0000	0.0000	0.0000
$\xi = 1.0$	2.1107	-6.6056	4.8527	5.5156	-14.8095	9.8225	0.0000	0.0000	0.0000

Table A6 Fit coefficients for the α^2 terms in the multidimensional parabolic fit for the drag coefficient produced by the airfoil sections of the CRM/uCRM wing as a function of angle of attack, Mach number, and Reynolds number.

	$a_{D,200}$	$a_{D,201}$	$a_{D,202}$	$a_{D,210}\times10^7$	$a_{D,211}\times10^7$	$a_{D,212}\times10^7$	$a_{D,220}$	$a_{D,221}$	$a_{D,222}$
$\xi = 0.0$	-29.3175	125.2950	-96.5283	-12.0835	31.1859	-19.7837	0.0000	0.0000	0.0000
$\xi = 0.1$	-38.2340	147.1626	-109.6929	-10.0881	26.6275	-17.1962	0.0000	0.0000	0.0000
$\xi = 0.15$	-39.8641	151.8656	-112.8863	-11.5079	30.4493	-19.7782	0.0000	0.0000	0.0000
$\xi = 0.2$	-41.8532	155.3432	-114.2371	-13.1423	34.4909	-22.2512	0.0000	0.0000	0.0000
$\xi = 0.25$	-39.9437	148.3293	-108.5422	-12.7401	33.6001	-21.7748	0.0000	0.0000	0.0000
$\xi = 0.3$	-44.7487	159.6118	-115.1512	-9.0101	24.1681	-15.8819	0.0000	0.0000	0.0000
$\xi = 0.35$	-50.0983	173.9021	-124.4604	2.0535	-5.7130	3.9051	0.0000	0.0000	0.0000
$\xi = 0.37$	-45.2050	162.1663	-117.8794	-12.1454	32.9826	-21.9460	0.0000	0.0000	0.0000
$\xi = 0.4$	-7.3546	52.8462	-40.6669	-60.1637	173.4676	-122.7107	0.0000	0.0000	0.0000
$\xi = 0.45$	-42.5019	155.0687	-113.7193	-12.5075	35.3122	-24.3604	0.0000	0.0000	0.0000
$\xi = 0.5$	-48.4733	172.0750	-125.6363	0.6943	-2.0402	1.4810	0.0000	0.0000	0.0000
$\xi = 0.55$	-52.5214	184.7772	-135.0893	1.7306	-4.9505	3.4937	0.0000	0.0000	0.0000
$\xi = 0.6$	-36.9600	140.6751	-104.1685	-10.0047	31.1780	-23.0141	0.0000	0.0000	0.0000
$\xi = 0.65$	-47.2434	170.4245	-125.6433	-11.8329	33.0339	-22.4416	0.0000	0.0000	0.0000
$\xi = 0.7$	-37.3132	141.1789	-104.6604	-29.4374	84.2729	-58.8640	0.0000	0.0000	0.0000
$\xi = 0.75$	-20.4532	91.6385	-69.2266	-62.8641	181.0406	-127.2507	0.0000	0.0000	0.0000
$\xi = 0.8$	-45.3995	165.2642	-122.0605	-17.1845	46.2002	-30.6045	0.0000	0.0000	0.0000
$\xi = 0.85$	-45.2908	163.5222	-119.9219	-12.0494	31.0498	-19.8488	0.0000	0.0000	0.0000
$\xi = 0.9$	-48.6533	172.4732	-125.8618	-8.7429	21.9033	-13.5197	0.0000	0.0000	0.0000
$\xi = 0.95$	-47.6118	169.3364	-123.4272	-18.0857	51.5001	-35.5157	0.0000	0.0000	0.0000
$\xi = 1.0$	-53.4387	183.5192	-132.0227	11.2253	-29.6558	19.8096	0.0000	0.0000	0.0000

Table A7 Location and thickness data for the leading-edge spar, trailing-edge spar, upper and lower skins, and ribs of the uCRM-9 wingbox geometry.

Section	ξ_{LE}	x_{LE}/c	t_{LE}, mm	h_{LE}, m	ξ_{TE}	x_{TE}/c	t_{TE}, mm	h_{TE}, m	t_{US}, mm	t_{LS}, mm	t_{rib}, mm
0	0.0000	0.2524	1.4396	2.0371	0.0000	0.6936	0.6517	1.2970	1.8226	2.0274	0.4526
1	0.0264	0.2178	1.2204	1.8564	0.0264	0.6730	0.6865	1.2942	1.9227	2.1048	0.4905
2	0.0527	0.1806	0.9505	1.6504	0.0527	0.6509	0.8352	1.2858	2.0233	2.1826	0.5402
3	0.0791	0.1407	0.9639	1.4163	0.0791	0.6272	1.0439	1.2711	2.1246	2.2609	0.5652
4	0.1055	0.0978	0.7299	1.1415	0.1055	0.6019	-	1.2473	1.7945	1.7093	1.2409
5	0.1258	0.1016	0.5576	1.0797	0.1055	0.2301	-	1.2438	1.8025	1.6849	0.4526
6	0.1462	0.1056	0.5620	1.0193	0.1055	0.3596	-	1.2407	1.8990	1.7610	0.4526
7	0.1665	0.1089	0.5608	0.9603	0.1055	0.4891	1.2544	1.2372	1.9048	1.8375	0.4526
8	0.1868	0.1123	0.5406	0.9049	0.1084	0.6026	0.8677	1.2320	1.8208	1.7735	0.4812
9	0.2072	0.1157	0.5333	0.8540	0.1310	0.6090	0.6028	1.1220	1.7238	1.6970	0.4724
10	0.2275	0.1193	0.5333	0.8072	0.1535	0.6157	0.5333	1.0316	1.6285	1.6210	0.4568
11	0.2478	0.1232	0.5333	0.7642	0.1760	0.6219	0.5333	0.9573	1.5728	1.5717	0.4526
12	0.2681	0.1274	0.5333	0.7250	0.1986	0.6286	0.5333	0.8916	1.6122	1.6478	0.4526
13	0.2885	0.1319	0.5333	0.6893	0.2211	0.6356	0.5333	0.8320	1.6603	1.7243	0.4526
14	0.3088	0.1369	0.5333	0.6568	0.2436	0.6432	0.5333	0.7777	1.7169	1.8012	0.4526
15	0.3291	0.1422	0.7333	0.6273	0.2662	0.6515	0.5496	0.7271	1.8043	1.8786	0.4526
16	0.3495	0.1481	1.1200	0.6009	0.2887	0.6607	0.7334	0.6788	1.8943	1.9564	0.5286
17	0.3698	0.1545	1.1316	0.5777	0.3112	0.6707	0.5401	0.6310	1.8988	2.0018	1.0926
18	0.3901	0.1570	0.7449	0.5639	0.3338	0.6818	0.5444	0.5817	1.9125	1.9734	0.7751
19	0.4104	0.1596	0.5937	0.5514	0.3563	0.6941	0.7333	0.5303	1.8404	1.8962	0.4709
20	0.4308	0.1579	0.6146	0.5398	0.3786	0.7016	0.7333	0.4903	1.7776	1.8195	0.5069
21	0.4511	0.1650	0.6208	0.5287	0.4004	0.7002	0.6165	0.4761	1.7498	1.7432	0.4526
22	0.4714	0.1680	0.6158	0.5174	0.4223	0.6988	0.5991	0.4635	1.7042	1.6782	0.4526
23	0.4918	0.1710	0.6120	0.5064	0.4441	0.6972	0.5984	0.4514	1.6480	1.6164	0.4526
24	0.5121	0.1742	0.6059	0.4967	0.4660	0.6957	0.5970	0.4400	1.5790	1.5490	0.4526
25	0.5324	0.1775	0.6047	0.4880	0.4878	0.6941	0.5967	0.4284	1.5092	1.4767	0.4526
26	0.5528	0.1810	0.6010	0.4797	0.5096	0.6924	0.5952	0.4171	1.4390	1.4025	0.4526
27	0.5731	0.1847	0.6332	0.4715	0.5315	0.6906	0.5978	0.4065	1.3698	1.3289	0.4526
28	0.5934	0.1886	0.5927	0.4634	0.5533	0.6888	0.5942	0.3964	1.2944	1.2556	0.4526
29	0.6137	0.1927	0.5908	0.4553	0.5752	0.6868	0.5891	0.3860	1.2179	1.1828	0.4526
30	0.6341	0.1970	0.5794	0.4472	0.5970	0.6848	0.5847	0.3755	1.1438	1.1105	0.4526
31	0.6544	0.2015	0.5719	0.4385	0.6189	0.6826	0.5794	0.3653	1.0954	1.0385	0.4526
32	0.6747	0.2063	0.5631	0.4291	0.6407	0.6804	0.5746	0.3555	1.0564	0.9670	0.4526
33	0.6951	0.2114	0.5555	0.4194	0.6626	0.6779	0.5680	0.3460	1.0253	0.8960	0.4526
34	0.7154	0.2168	0.5489	0.4098	0.6844	0.6754	0.5616	0.3370	0.9923	0.8254	0.4526
35	0.7357	0.2226	0.5438	0.4002	0.7063	0.6726	0.5549	0.3284	0.9589	0.7552	0.4526
36	0.7560	0.2287	0.5333	0.3904	0.7281	0.6697	0.5470	0.3199	0.9192	0.6854	0.4526
37	0.7764	0.2353	0.5333	0.3805	0.7500	0.6666	0.5393	0.3109	0.8800	0.6162	0.4526
38	0.7967	0.2423	0.5333	0.3703	0.7718	0.6633	0.5333	0.3005	0.8378	0.5691	0.4526
39	0.8170	0.2498	0.5333	0.3599	0.7936	0.6597	0.5333	0.2894	0.7925	0.5337	0.4526
40	0.8374	0.2579	0.5333	0.3492	0.8155	0.6558	0.5333	0.2786	0.7437	0.4982	0.4526
41	0.8577	0.2666	0.5333	0.3382	0.8373	0.6516	0.5333	0.2682	0.6949	0.4574	0.4526
42	0.8780	0.2760	0.5333	0.3269	0.8592	0.6470	0.5333	0.2583	0.6566	0.4153	0.4526
43	0.8984	0.2862	0.5333	0.3154	0.8810	0.6420	0.5333	0.2487	0.6114	0.3772	0.4526
44	0.9187	0.2973	0.5333	0.3038	0.9029	0.6365	0.5333	0.2386	0.5600	0.3762	0.4526
45	0.9390	0.3094	0.5333	0.2922	0.9247	0.6303	0.5333	0.2276	0.5086	0.3751	0.4526
46	0.9593	0.3209	0.5333	0.2808	0.9466	0.6236	0.5333	0.2167	0.4971	0.3741	0.4526
47	0.9797	0.3373	0.5333	0.2691	0.9684	0.6163	0.5333	0.2062	0.4956	0.3730	0.4526
48	1.0000	0.3536	0.5333	0.2560	1.0000	0.6039	0.5333	0.1890	0.4956	0.3730	0.4526

Table A8 Approximations for the locus of centers of gravity, elastic axis, and flexural and torsional stiffness of the uCRM-9 wingbox geometry.

section	ξ	x_{cg}/c	x_{ea}/c [24]	x_{ea}/c [41]	x_{ea}/c [42]	x_{ea}/c (avg)	EI, N.m^2×10^{-9}	GJ, N.m^2/rad ×10^{-9}
0	0.0000	0.4507	0.4214	-	-	0.4214	10.0052	7.6883
1	0.0264	0.4287	0.4024	-	-	0.4024	9.2733	7.2357
2	0.0527	0.4057	0.3844	-	-	0.3844	10.8361	7.6534
3	0.0791	0.3798	0.3690	-	-	0.3690	9.2963	6.6712
4	0.1055	0.3677	0.3595	0.4046	0.4071	0.3904	7.4630	5.0283
5	0.1139	0.3648	0.3709	0.4070	0.4121	0.3967	6.8888	4.6576
6	0.1212	0.3622	0.3808	0.4091	0.4165	0.4021	6.4375	4.3570
7	0.1295	0.3592	0.3921	0.4115	0.4185	0.4074	6.0379	4.1393
8	0.1416	0.3305	0.4086	0.4153	0.4210	0.4150	5.4871	3.8367
9	0.1639	0.3812	0.4097	0.4216	0.4265	0.4193	4.7280	3.3576
10	0.1860	0.3829	0.4116	0.4279	0.4324	0.4240	4.1395	2.9743
11	0.2079	0.3873	0.4147	0.4345	0.4354	0.4282	3.5313	2.5800
12	0.2298	0.3928	0.4182	0.4415	0.4413	0.4337	2.6721	2.1271
13	0.2516	0.3988	0.4221	0.4490	0.4469	0.4393	2.2503	1.8254
14	0.2735	0.4053	0.4265	0.4572	0.4533	0.4457	2.0076	1.6216
15	0.2953	0.4117	0.4311	0.4662	0.4620	0.4531	1.7067	1.4146
16	0.3172	0.4174	0.4358	0.4760	0.4751	0.4623	1.4977	1.2288
17	0.3392	0.4174	0.4403	0.4867	0.4845	0.4705	1.2962	1.0718
18	0.3615	0.4229	0.4424	0.4988	0.4972	0.4794	1.2084	0.9685
19	0.3839	0.4398	0.4351	0.5022	0.5043	0.4805	1.0475	0.8555
20	0.4059	0.4399	0.4237	0.4999	0.5056	0.4764	0.9188	0.7550
21	0.4271	0.4392	0.4255	0.4975	0.5064	0.4765	0.7754	0.6575
22	0.4482	0.4392	0.4256	0.4950	0.4987	0.4731	0.6820	0.5923
23	0.4693	0.4397	0.4257	0.4924	0.4939	0.4707	0.6197	0.5360
24	0.4904	0.4404	0.4258	0.4897	0.4895	0.4683	0.5735	0.4874
25	0.5116	0.4412	0.4255	0.4868	0.4849	0.4657	0.5247	0.4450
26	0.5327	0.4418	0.4252	0.4838	0.4801	0.4630	0.4615	0.3963
27	0.5538	0.4423	0.4252	0.4807	0.4789	0.4616	0.3986	0.3541
28	0.5749	0.4431	0.4252	0.4774	0.4757	0.4594	0.3355	0.3142
29	0.5961	0.4440	0.4253	0.4739	0.4715	0.4569	0.2917	0.2778
30	0.6172	0.4449	0.4254	0.4702	0.4672	0.4542	0.2601	0.2500
31	0.6383	0.4458	0.4257	0.4663	0.4591	0.4504	0.2088	0.2111
32	0.6593	0.4468	0.4265	0.4622	0.4477	0.4454	0.1864	0.1835
33	0.6804	0.4479	0.4275	0.4578	0.4381	0.4411	0.1453	0.1533
34	0.7014	0.4489	0.4287	0.4532	0.4343	0.4387	0.1243	0.1269
35	0.7224	0.4501	0.4302	0.4482	0.4386	0.4390	0.1033	0.1146
36	0.7435	0.4513	0.4319	0.4430	0.4305	0.4351	0.0932	0.1024
37	0.7645	0.4524	0.4335	0.4374	0.4176	0.4295	0.0716	0.0796
38	0.7855	0.4537	0.4349	0.4314	0.4034	0.4232	0.0621	0.0674
39	0.8066	0.4550	0.4363	0.4250	0.3904	0.4172	0.0621	0.0536
40	0.8277	0.4564	0.4380	0.4180	0.3874	0.4145	0.0397	0.0402
41	0.8487	0.4582	0.4401	0.4105	0.3734	0.4080	0.0311	0.0327
42	0.8697	0.4600	0.4427	0.4024	0.3658	0.4036	0.0311	0.0299
43	0.8907	0.4620	0.4457	0.3936	0.3630	0.4008	0.0311	0.0170
44	0.9117	0.4642	0.4489	0.3841	0.3530	0.3953	0.0311	0.0146
45	0.9328	0.4666	0.4521	0.3736	0.3401	0.3886	0.0311	0.0134
46	0.9538	0.4692	0.4547	0.3620	0.3259	0.3809	0.0311	0.0107
47	0.9748	0.4723	0.4600	0.3493	0.3025	0.3706	0.0311	0.0095
48	1.0000	0.4764	0.4597	0.3322	0.2708	0.3542	0.0311	0.0080

Acknowledgements

This material is partially based upon work supported by NASA under Grant No. 80NSSC18K1696 issued by the Aeronautics Research Mission Directorate through the 2018 NASA Fellowship Activity with Nhan Nguyen as the NASA Technical Advisor.

References

[1] Vassberg, J. C., DeHaan, M. A., Rivers, S. M., and Wahls, R. A., "Development of a Common Research Model for Applied CFD Validation Studies," AIAA 2008-6919, 26th AIAA Applied Aerodynamics Conference, Honolulu, HI, 18-21 August 2008. (doi:10.2514/6.2008-6919)

[2] Vassberg, J. C., DeHaan, M. A., Rivers, S. M., and Wahls, R. A., "Retrospective on the Common Research Model for Computational Fluid Dynamics Validation Studies," *Journal of Aircraft*, Vol. 55, No. 4, 2018, pp. 1325-1337. (doi:10.2514/1.C034906)

[3] Rivers, M. B. and Dittberner, A., "Experimental Investigation of the NASA Common Research Model (Invited)," AIAA 2010-4218, 28th AIAA Applied Aerodynamics Conference, Chicago, IL, 28 June-1 July 2010. (doi:10.2514/6.2010-4218)

[4] Rivers, M. B., Quest, J., and Rudnik, R., "Comparison of the NASA Common Research Model European Transonic Wind Tunnel Test Data to NASA Test Data (Invited)," AIAA 2015-1093, 53rd AIAA Aerospace Sciences Meeting, Kissimmee, FL, 5-9 January 2015. (doi:10.2514/6.2015-1093)

[5] Rivers, M. B., "NASA Common Research Model: A History and Future Plans," AIAA 2019-3725, AIAA Aviation 2019 Forum, Dallas, TX, 17-21 June 2019. (doi:10.2514/6.2019-3725)

[6] Development of the High Lift Common Research Model (HL-CRM): A Representative High Lift Configuration for Transonic Transports," AIAA 2016-0308, 24th AIAA Aerospace Sciences Meeting, San Diego, CA, 4-8 January 2016. (doi:10.2514/6.2016-0308)

[7] Lynde, M. N. and Campbell, R. L., "Computational Design and Analysis of a Transonic Natural Laminar Flow Wing for a Wind Tunnel Model," AIAA 2017-3058, 35th AIAA Applied Aerodynamics Conference, Denver, CO, 5-9 June 2017. (doi:10.2514/6.2017-3058)

[8] Rivers, M. B., Lynde, M. N., Campbell, R. L., Viken, S. A., Chan, D. T., Watkins, A. N., and Goodliff, S. L., "Experimental Investigation of the NASA Common Research Model with a Natural Laminar Flow Wing in the NASA Langley National Transonic Facility," AIAA 2019-2189, AIAA SciTech 2019 Forum, San Diego, CA, 7-11 January 2019. (doi:10.2514/6.2019-2189)

[9] Lynde, M. N., Campbell, R. L., and Viken, S. A., "Additional Findings from the Common Research Model Natural Laminar Flow Wind Tunnel Test," AIAA 2019-3292, AIAA Aviation 2019 Forum, Dallas, TX, 17-21 June 2019. (doi:10.2514/6.2019-3292)

[10] Atinault, O. and Hue, D., "Design of a vertical tail for the CRM configuration," ONERA RT 1/21960 GMT/DAAP, June 2014.

[11] Cartieri, A., Hue, D., Chanzy, Q., and Atinault, O., "Experimental Investigations on the Common Research Model at ONERA-SIMA – Comparison with DPW Numerical Results," AIAA 2017-0964, 55th AIAA Aerospace Sciences Meeting, Grapevine, TX, 9-13 January 2017, (doi:10.2514/6.2017-0964)

[12] Ueno, M., Kohzai, T., Koga, S., Kato, H., Nakakita, K., and Sudani, N., "80% Scaled NASA Common Research Model Wind Tunnel Tests in JAXA," AIAA 2013-0963, 51st AIAA Aerospace Sciences Meeting, Grapevine, TX., 7-10 January 2013. (doi:10.2514/6.2013-0963)

[13] Broughton, C. A., Bendmeddour, A., Mebarki, Y., and Rivers, M. B., "Experimental Investigations of the NASA common Research Semispan Model in the NRC 5-Foot Trisonic Wind Tunnel," AIAA 2018-4285, 2018 Aerodynamic Measurement Technology and Ground Testing Conference, Atlanta, GA, 25-29 June 2018. (doi:10.2514/6.2018-4285)

[14] Klimmek, T., "Development of a Structural Model of the CRM Configuration for Aeroelastic and Loads Analysis," *International Forum on Aeroelasticity and Structural Dynamics*, Royal Aeronautical Society., Bristol, England, U.K., June 2013, Paper 1794.

[15] Kennedy, G. J., Kenway, G. W., and Martins, J. R. R. A., "High Aspect Ratio Wing Design: Optimal Aerostructural Tradeoffs for the Next Generation of Materials," AIAA 2014-0596, 52nd Aerospace Sciences Meeting, National Harbor, MD, 13-17 January 2014. (doi:10.2514/6.2014-0596)

[16] Brooks, T. R., Kenway, G. K. W., and Martins, J. R. R. A., "Benchmark Aerostructural Models for the Study of Transonic Aircraft Wings," *AIAA Journal*, Vol. 56, No. 7, July 2018 pp. 2840- 2855. (doi:10.2514/1.J056603)

[17] Keye, S. Brodersen, O., and Rivers, M. B., "Investigation of Aeroelastic Effects on the NASA Common Research Model," *Journal of Aircraft*, Vol, 51, No. 4, July-August 2014, pp. 1323-1330. (doi:10.2514/1.C032598)

[18] Vassberg, J. C., Tinoco, E. N., Mani, M., Rider, B., Zickuhr, T., Levy, D. W., Brodersen, O. P., Eisfeld, B., Crippa, S., Wahls, R. A., Morrison, J. H., Mavriplis, D. J., and Murayama, M., "Summary of the Fourth AIAA Computational Fluid Dynamics Drag Prediction Workshop," *Journal of Aircraft*, Vol. 51, No. 4, July-August 2014, pp. 1070-1089. (doi:10.2514/1.C032418)

[19] Keye, S. and Brodersen, O., "Investigations of Fluid-Structure Coupling and Turbulence Model Effects on the DLR Results of the Fifth AIAA CFD Drag Prediction Workshop", AIAA 2013-2509, 31st AIAA Applied Aerodynamics Conference, San Diego, CA, 24-27 June 2013. (doi:10.2514/6.2013-2509)
[20] Morrison, J., "Statistical Analysis of CFD Solutions From the Fifth AIAA Drag Prediction Workshop." AIAA 2013-47, 51st AIAA Aerospace Sciences Meeting, Grapevine, TX, 7-10 January 2013. (doi:10.2514/6.2013-47)
[21] Tinoco, E. N., Brodersen, O. P., Keye, S., Laflin, K. R., Feltrop, E., Vassberg, J. C., Mani, M., Rider, B., Wahls, R. A., Morrison, J. H.., Hue, D., Roy, C. J., Mavriplis, D. J., and Murayama, M., "Summary Data from the Sixth AIAA CFD Drag Prediction Workshop: CRM Cases," *Journal of Aircraft*, Vol. 55, No. 4, July-August 2018, pp. 1352-1379. (doi:10.2514/1.C034409)
[22] Keye, S. and Mavriplis, D., "Summary of Case 5 from Sixth Drag Prediction Workshop: Coupled Aerostructural Simulation," *Journal of Aircraft*, Vol. 55, No. 4, July-August 2018, pp. 1380-1387. (doi:10.2514/1.C034427)
[23] Hue, D., Chanzy, Q., and Landier, Sâm, "DPW-6: Drag Analyses and Increments Using Different Geometries of the Common Research Model Airliner," *Journal of Aircraft*, Vol. 55, No. 4, July-August 2018, pp. 1509-1521. (doi:10.2514/1.C034139)
[24] Chauhan, S. S. and Martins, J. R. R. A., "Low-fidelity aerostructural optimization of aircraft wings with a simplified wingbox model using OpenAeroStruct," *Proceedings of the 6th International Conference on Engineering Optimization*, EngOpt 2018, pp. 418-431. (doi:10.1007/978-3-319-97773-7_38)
[25] Wiberg, B. D., Fujiwara, G. E. C., Woodard, B., and Bragg, M., "Large-Scale Swept-Wing Icing Simulations in the NASA Glenn Icing Research Tunnel Using LEWICE3D," AIAA 2014-2617, 6th AIAA Atmospheric and Space Environments Conference, Atlanta, GA, 16-20 June 2014. (doi:10.2514/6.2014-2617)
[26] Koivisto, P., Soinne, E., and Kivekäs, J., "Anti-Icing Fluid Secondary Wave and Its Role in Lift Loss During Takeoff," *Journal of Aircraft*, Vol. 55, No. 6, November-December 2018, pp. 2298-2306. (doi:10.2514/1.C034694)
[27] Stanford, B. K. and Massey, S. J., "Uncertainty Quantification of the FUN3D-Predicted NASA CRM Flutter Boundary," AIAA 2017-1816, 58th AIAA/ASCE/AHS/ASC Structures, Structural Dynamics, and Materials Conference, Grapevine TX, 9-13 January 2017. (doi:10.2514/6.2017-1816)
[28] Fujiwara, G. E. C., Nguyen, N. T., Livne, E., and Bragg, M. B., "Aerostructural Design Optimization of a Flexible Wing Aircraft with Continuous Morphing Trailing Edge," AIAA 2018-3517, 2018 Multidisplinary Analysis and Optimization Conference, Atlanta, GA, 25-29 June 2018. (doi:10.2514/6.2018-3517)
[29] Phillips, W. F., "Lifting-Line Analysis for Twisted Wings and Washout-Optimized Wings," *Journal of Aircraft*, Vol. 41, No. 1, 2004, pp. 128–136. (doi:10.2514/1.262)
[30] Phillips, W. F., Fugal, S. R., and Spall, R. E., "Minimizing Induced Drag with Wing Twist, Computational-Fluid-Dynamics Validation," *Journal of Aircraft*, Vol. 43, No. 2, 2006, pp. 437–444. (doi:10.2514/1.15089)
[31] Gallay, S., and Laurendeau, E., "Preliminary-Design Aerodynamic Model for Complex Configurations Using Lifting-Line Coupling Algorithm," *Journal of Aircraft*, Vol. 53, No. 4, 2016, pp. 1145–1159. (doi:10.2514/1.C033460)
[32] Phillips, W. F., and Hunsaker, D. F., "Lifting-Line Predictions for Induced Drag and Lift in Ground Effect," *Journal of Aircraft*, Vol. 50, No. 4, 2013, pp. 1226–1233. (doi:10.2514/1.C032152)
[33] Wickenheiser, A., and Garcia, E., "Aerodynamic Modeling of Morphing Wings Using an Extended Lifting-Line Analysis," *Journal of Aircraft*, Vol. 44, No. 1, 2007, pp. 10–16. (doi:10.2514/1.18323)
[34] Phillips, W. F., and Snyder, D. O., "Modern Adaptation of Prandtl's Classic Lifting-Line Theory," *Journal of Aircraft*, Vol. 37, No. 4, 2000, pp. 662–670. (doi:10.2514/2.2649)
[35] Rasmussen, M. L., and Smith, D. E., "Lifting-Line Theory for Arbitrarily Shaped Wings," *Journal of Aircraft*, Vol. 36, No. 2, 1999, pp. 340–348. (doi:10.2514/2.2463)
[36] Bera, R. K., "Some remarks on the solution of the lifting line equation," *Journal of Aircraft*, Vol. 11, No. 10, 1974, pp. 647–648. (doi:10.2514/3.44397)
[37] Prandtl, L., "Tragflügel Theorie," *Nachricten von der Gesellschaft der Wissenschaften zu Göttingen*, Geschäeftliche Mitteilungen, Klasse, 1918, pp. 451–477.
[38] Prandtl, L., "Applications of Modern Hydrodynamics to Aeronautics," NACA TR-116, June 1921.
[39] Fujiwara, G. E. C., Chaparro, D., and Nguyen, N., "An Integral Boundary Layer Direct Method Applied to 2D Transonic Small-Disturbance Equations," AIAA 2016-3568, 34th AIAA Applied Aerodynamics Conference, Washington, D. C., 13-17 June 2016. (doi:10.2514/6.2016-3568)
[40] Ullah, A. H., Fabijanic, C., Estevadeordal, J., Montgomery, Z. S., Hunsaker, D. F., Staiger, J. M., and Joo, J. J., "Experimental and Numerical Evaluation of the Performance of Parabolic Flaps," AIAA 2019-2916, AIAA Aviation 2019 Forum, Dallas, Texas, 17-21 June 2019. (doi:10.2514/6.2019-2916)
[41] Cramer, N. B. and Nguyen, N. T., "Development of an Aeroservoelastic Model for Gust Load Alleviation of the NASA Common Research Model Wind Tunnel Experiment," AIAA 2020-0211, AIAA SciTech 2020 Forum, Orlando, Florida, 6-10 January 2020. (doi:10.2514/6.2020-0211)
[42] Stodieck, O., Cooper, J. E., and Weaver, P. M., "Interpretation of Bending/Torsion Coupling for Swept, Nonhomogenous Wings," *Journal of Aircraft*, Vol. 53, No. 4, 2016, pp. 892-899. (doi:10.2514/1.C033186)

[43] “777-200/300 Airplane Characteristics for Airport Planning”, D6-58329, Boeing Commercial Airplanes, July, 1998.
[44] “Boeing 777 Airplane Rescue and Fire Fighting Information,” Boeing Commercial Airplanes, October, 2018.
[45] Taylor, J. D. and Hunsaker, D. F., “Numerical Method for Rapid Aerostructural Design and Optimization,” AIAA 2020-3175, AIAA Aviation 2020 Virtual Forum, 15-19 June, 2020. (doi:10.2514/6.2020-3175)
[46] Reid, J. T., and Hunsaker, D. F., “A General Approach to Lifting-Line Theory, Applied to Wings with Sweep,” AIAA 2020-1287, AIAA SciTech 2020 Forum, Orlando, Florida, 6-10 January, 2020. (doi:10.2514/6.2020-1287)
[47] Lyu, Z., Kenway, G. K., and Martins, J. R. R. A., “RANS-based Aerodynamic Shape Optimization Investigations of the Common Research Model Wing,” AIAA 2014-0567, 52nd Aerospace Sciences Meeting, National Harbor, Maryland, 13-17 January, 2014. (doi:10.2514/6.2014-0567)